Neurobiology of Disease 124 (2019) 563–572

Contents lists available at ScienceDirect

Neurobiology of Disease

journal homepage: www.elsevier.com/locate/ynbdi

Local cortical circuit correlates of altered EEG in the mouse model of Fragile X syndrome

Sonal Goswami, Sheridan Cavalier, Vinay Sridhar, Kimberly M. Huber*, Jay R. Gibson*

Department of Basic Neuroscience, University of Texas Southwestern Medical Center, Dallas, TX 75390, United States

ARTICLE INFO

Keywords:
Fragile X
Cortex
Hyperexcitability
Gamma
Synchrony
EEG

ABSTRACT

Electroencephalogram (EEG) recordings in Fragile X syndrome (FXS) patients have revealed enhanced sensory responses, enhanced resting "gamma frequency" (30–100 Hz) activity, and a decreased ability for sensory stimuli to modulate cortical activity at gamma frequencies. Similar changes are observed in the FXS model mouse – the *Fmr1* knockout. These alterations may become effective biomarkers for diagnosis and treatment of FXS. Therefore, it is critical to better understand what circuit properties underlie these changes. We employed Channelrhodopsin2 to optically activate local circuits in the auditory cortical region in brain slices to examine how changes in local circuit function may be related to EEG changes. We focused on layers 2/3 and 5 (L2/3 and L5). In *Fmr1* knockout mice, light-driven excitation of L2/3 revealed hyperexcitability and increased gamma frequency power in both local L2/3 and L5 circuits. Moreover, there is increased synchrony in the gamma frequency band between L2/3 and L5. Hyperexcitability and increased gamma power were not observed in L5 with L5 light-driven excitation, indicating that these changes were layer-specific. A component of L2/3 network hyperexcitability is independent of ionotropic receptor mediated synaptic transmission and may be mediated by increased intrinsic excitability of L2/3 neurons. Finally, lovastatin, a candidate therapeutic compound for FXS that targets ERK signaling did not normalize changes in gamma activity. In conclusion, hyperactivity and increased gamma activity *in* local neocortical circuits, together with increased gamma synchrony *between* circuits, provide a putative substrate for EEG alterations observed in both FXS patients and the FXS mouse model.

1. Introduction

Fragile X syndrome (FXS) is the leading cause of intellectual disability and the most common monogenic form of autism (Bassell and Warren, 2008; Abrahams and Geschwind, 2008). Patients with FXS present with cognitive and social deficits, autistic characteristics, seizures, sensory hypersensitivity, and hyperactivity (Hagerman et al., 2009; Berry-Kravis, 2002). Many of these impairments are reproduced in the FXS mouse model, the *Fmr1* knockout (KO) mouse (Bakker, 1994; Miller et al., 1999; Musumeci et al., 2000; Nielsen et al., 2002; Spencer et al., 2005; Brennan et al., 2006).

Behavioral and functional measurements in FXS patients suggest that neural circuits are hyperexcitable. For example, seizures are reported in 10–20% of patients (Berry-Kravis, 2002; Musumeci et al., 1999) and many display sensory hypersensitivity (Miller et al., 1999; Baranek et al., 2008). Electrophysiological measurements, mainly in the form of the electroencephalogram (EEG), show enhanced sensory responses (Knoth et al., 2014; Castren et al., 2003; Rojas et al., 2001; Van der Molen et al., 2011). Finally, spontaneous activity in the cortex of FXS patients appears increased since EEG signals in the gamma range (30–80 Hz) are increased under resting state conditions (Wang et al., 2017).

Recent studies in FXS patients investigating event-related potentials (ERPs) in the auditory system indicate that they are larger (Knoth et al., 2014; Van der Molen et al., 2012), and their habituation (response decrement with repeated stimuli) is reduced compared to control individuals (Ethridge et al., 2016; Schneider et al., 2013). And while resting state power in the gamma frequency range is increased, the ability of auditory stimuli to synchronize and phase-lock cortical activity at gamma frequencies is decreased (Ethridge et al., 2016, 2017). These changes provide potential biomarkers for diagnosis and treatment of FXS.

Similar alterations have been reported in the auditory system of the FXS mouse model – the *Fmr1* knockout (KO). Electrophysiological responses to both somatosensory and auditory stimuli are increased (Zhang et al., 2014; Rotschafer and Razak, 2013), and habituation to repeated auditory stimuli is deficient when compared to wild-type (WT) mice (Lovelace et al., 2016). Recent work finds, as in patients, resting

* Corresponding authors.
E-mail addresses: Kimberly.Huber@UTSouthwestern.edu (K.M. Huber), Jay.Gibson@UTSouthwestern.edu (J.R. Gibson).

https://doi.org/10.1016/j.nbd.2019.01.002
Received 20 August 2018; Received in revised form 1 January 2019; Accepted 5 January 2019
Available online 09 January 2019
0969-9961/

state EEG power is increased in the gamma frequency range, but the ability of auditory stimuli to synchronously drive cortical activity in the gamma range is decreased (Lovelace et al., 2018; Sinclair et al., 2017). Because of the remarkable conservation of EEG phenotypes between patients and the *Fmr1* KO mouse model, identification of the circuit mechanisms underlying the EEG changes in the *Fmr1* KO mouse may be highly relevant to those that occur in FXS patients.

The mechanisms for the above systems level changes are unknown, and it is not known if changes in neocortex, itself, play a role. Many cellular and synaptic alterations occur in the neocortex of *Fmr1* KO mice, but their role in these neural network level changes remains unclear (Contractor et al., 2015; Wang et al., 2014; Darnell et al., 2011; Darnell and Klann, 2013; Patel et al., 2014). We argue that extracellular measurements of activity provide a more direct link to EEG related signals since EEG signals are extracellular and generated at the population level in the neocortex (Luck, 2005). Therefore, we investigated functional alterations in the auditory cortical region of the *Fmr1* KO mouse using extracellular recordings of local network activity induced by channelrhodopsin2-mediated (ChR2-mediated) depolarization of neurons. We tested the hypothesis that local cortical circuit alterations and changes in synchrony among circuits are potential substrates for the EEG alterations in FXS.

In slices obtained from *Fmr1* knockout mice, we find changes in auditory cortical regions that are consistent with the system level changes described above. Cortical circuits are hyperexcitable and display changes in gamma activity and gamma synchrony that are consistent, and correlate, with alterations in the EEG. These findings provide the first step to understanding the mechanisms of potential EEG biomarkers for brain function in FXS.

2. Methods and materials

2.1. Mice

Female mice heterozygous for *Fmr1* (“sighted” FVB strain; Jackson Labs, #004828) (Bakker, 1994) and homozygous for a floxed *channelrhodopsin* (Ai32, ChR2 (H134R)-EYFP, Jackson Labs, #024109) (Madisen et al., 2012), were crossed with homozygous vGlut2-IRES-Cre males (Slc17a6$^{tm2(cre)Lowl}$/J, Jackson Labs #016963) (Vong et al., 2011). This resulted in male *Fmr1* KO and littermate WT controls expressing ChR2 in excitatory glutamate-releasing neurons. All experimental procedures were approved by the Institutional Animal Care and Use Committee at the University of Texas Southwestern Medical Center.

2.2. Extracellular recordings in slices

Coronal slices were prepared from P19-23 male mice in a similar manner as described before (Hays et al., 2011). Wild-type (WT) and *Fmr1* KO mice were anesthetized with a mixture of ketamine (125 mg/kg) and xylazine (25 mg/kg). Brains were rapidly removed and placed in partially frozen modified ACSF containing the following (in mM): 84 NaCl, 3 KCl, 1.25 NaH2PO4, 7 MgSO4, 0.5 CaCl, 26 NaHCO3, 20 Glucose, 70 Sucrose, 1 kynurenic acid. Coronal slices containing the auditory cortex (400 μm) were prepared using a Leica 1200VS vibratome. Slices recovered at 30 degrees on an interface chamber (Harvard apparatus) for 1 h while being perfused with a low activity buffer (2 min/ml) containing the following (in mM): 126 NaCl, 3 KCl, 1.25 NaH2PO4, 2 MgSO4, 2 CaCl, 26 NaHCO3, 25 Glucose. Slices recovered for an additional hour in physiological ACSF containing (in mM): 126 NaCl, 3.5 KCl, 1.25 NaH2PO4, 1.2 MgSO4, 1.2 CaCl, 26 NaHCO3, 15 Glucose. Recordings followed in the same physiological saline.

Auditory cortex was identified using two landmarks - the presence of dorsal and ventral hippocampus and the rhinal fissure. Tungsten recording electrodes (< 0.5 MΩ, FHC) were placed 1 mm dorsal to the rhinal fissure. We did not precisely identify primary auditory cortex using the thalamocortical slice (Cruikshank et al., 2002) because the number of slices in which this identification was possible was 10% of all slices, and therefore, was prohibitive in obtaining sufficient sample numbers. Recordings were performed in ACSF at 30 °C. Signals were amplified 10,000 times using a DC amplifier (A-M systems model 1800) and sampled at 5000 Hz (National Instruments). For 500 and 1500 ms light applications, a 1–5000 Hz hardware filter was applied. For 10 ms light application, a 100–5000 Hz hardware filter was applied to prevent saturation.

2.3. Light stimuli

An LED fiberoptic light (Mightex Systems) applied 473 nm light in a 350 um diameter circle. Intensity was computer-controlled through a LED driver (Mightex Systems). There were 4 types of light stimuli: 1) 10 ms step, 2) 500 ms exponentially increasing ramp, 3) 1500 ms exponentially increasing ramp, and 4) 1000 ms sinewave stimulus of exponentially increasing amplitude.

Details for light stimuli above are as follows (in corresponding order):

1) *10 ms step* of a constant intensity (I),
2) *500 ms light ramp* with a temporal intensity profile of $K*(1 + 0.2*(1-e^{-t/\tau}))$ and $\tau = 80$ ms. The stated intensity for this ramp is the final steady state, $I = 1.2*K$. For initial experiments, 2 intensities were applied – 0.25 mW/mm^2 and 0.35 mW/mm^2. For light applied directly to layer 5, intensities were 0.09, 0.2, and 0.35 mW/mm^2. For each of these experiments, we limited our analysis to responses to the highest light intensity because this produced the most reliable differences in *Fmr1* KO slices.
3) *1500 ms light ramp* with temporal intensity profile of $K*(1 + 4*(1-e^{-t/\tau}))$ and $\tau = 160$ ms. Again, the intensity stated is the final steady state, $I = 5*K$. For initial experiments, 2 intensities were applied – 0.25 mW/mm^2 and 0.35 mW/mm^2. For the same reasons as stated above in item 2, only the data from the highest intensity will be presented.
4) *1000 ms sinewave* stimulus. A 700 ms sinewave stimulus was superimposed on a 1000 ms ramp with a temporal profile of $K*(1 + 2*(1-e^{-t/\tau}))$ after a 50 ms delay. The sinewave was exponentially increased in intensity as follows: $K*0.7 * 2*(1-e^{-t/\tau})$. $\tau = 160$ ms for both waveforms. The final steady state after the sinewave ended was $I = 3*K = 0.21$ mW/mm^2. The maximum sinewave amplitude was 0.2 mW/mm^2.

These light stimuli activated ChR2-mediated inward currents (Boyden et al., 2005) which were restricted to excitatory, glutamatergic neurons. The inward current depolarized these neurons and induced circuit activity. The exponentially increasing (or “ramping”) components were applied to compensate for ChR2-mediated current adaptation and for any adaptations to circuit function.

2.4. Analysis – time domain

Traces were processed in the following order: high-pass filtered with a 300 Hz lower cut-off frequency, rectified, box filtered based on 7 nearest neighbors, and baselines aligned (based on 120–20 ms before light application). Analysis windows for 10, 500, and 1500 ms light stimuli were chosen to avoid contamination by ChR2-mediated currents (Supp. data, *Determining Analysis Windows*) and to focus on times of maximal network activity. They were (with respect to light onset): 7–47 ms, 7–500 ms, and 40–1000 ms. Response amplitude was the average activity in these time windows minus the baseline activity (determined in the 100 ms window before light onset). Therefore, the response is not a peak. Average activity was chosen because it was less variable compared to peak.

2.5. Analysis – frequency domain

We examined the 30–100 Hz and 200–600 Hz frequency bands. Just as for the time-domain analysis, we chose analysis windows that avoid contamination by ChR2-mediated currents and to measure maximum activity (Supp. Data, *Determining Analysis Windows*). They were 10–500 ms and 40–1000 ms for 500 ms and 1500 ms ramps, respectively. While the sinewave was applied for 700 ms, we only analyzed the last half since the sine amplitude was bigger in that interval and produced the most robust effects. Power in the above bands is derived from the signal in the whole analysis window.

Normalized cross-correlograms were derived by dividing the raw correlogram by the product of the standard deviations of each trace (Deans et al., 2001). This function is largely independent of the total activity in each recording and has been previously employed to measure synchrony of neural activity (Deans et al., 2001; Gibson et al., 2008).

2.6. Compounds

The following compounds were used: (±)-3-(2-Carboxypiperazin-4-yl) propyl-1-phosphonic acid (CPP, Sigma), picrotoxin (Sigma), 6,7-Dinitroquinoxaline-2,3-dione disodium salt (DNQX, Tocris), tetrodotoxin (TTX, Sigma), cadmium chloride ($CdCl_2$, Sigma), lovastatin sodium salt (lovastatin, Sigma).

2.7. Statistics

Values are stated as the mean and the standard error of the mean (SEM). Sample numbers N refer to slice number, and in the results, an additional number is provided in parentheses to indicate the number of mice from which the slices were obtained (*e.g.* $N = 41(6)$). A single recording experiment was performed for each slice. On average, we obtained 5 slices per mouse. Values and N's are stated in WT, *Fmr1* KO order unless stated otherwise.

For power spectra (frequency-domain analysis), data were not normally distributed. When comparing just 2 groups, a non-parametric Mann-Whitney (M-W) *t*-test was applied. For consistency and clarity, we applied an M-W method for all *t*-tests. For ANOVAs performed on power spectra, the data were transformed by $\log_{10}$ to obtain normal distributions. But figures and text use linear means. Power values in scatterplots were plotted on $\log_{10}$ scales, but the mean superimposed on the individual points was a linear mean. Therefore, the means are skewed upward relative to the distribution plotted. For all ANOVAs, Sidak's multiple comparison tests were performed when necessary. In Fig. 8B, the data were square-root transformed to normalize the distribution. The M-W *t*-test and 2-way ANOVAs were performed using Graphpad Prism while 3-way ANOVAs were performed using SPSS Statistics (IBM). An rmANOVA indicates repeated measures.

3. Results

3.1. Local stimulation of L2/3 evokes activity that can be separated into 2 components

We induced layer 2/3 (L2/3) network activity by focal light activation of ChR2-mediated currents in glutamatergic neurons and measured this with extracellular recordings in L2/3 (Fig. 1A). Light stimuli were 500 and 1500 ms ramps (Fig. 1B). We first determined the relative contribution of synaptic potentials, action potentials, and ChR2-mediated currents to evoked activity by applying 2 different drug manipulations. We examined this in terms of the power spectrum of the activity generated, and focused on two frequency bands: 30–100 Hz and 200–600 Hz. We refer to the 30–100 Hz band as "gamma" as in previous studies (Wang et al., 2017; Lovelace et al., 2018) and the 200–600 Hz band as "high-frequency".

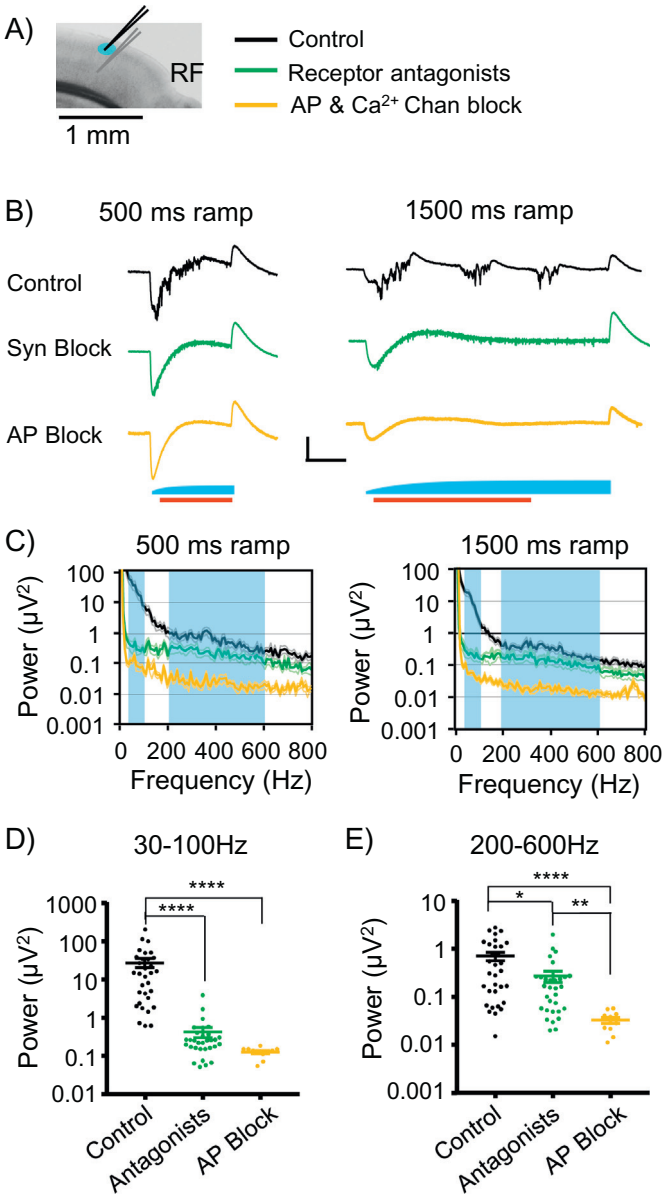

Fig. 1. Extracellularly recorded responses can be divided into two components. A) Schematic showing a coronal slice containing the auditory cortex. Blue indicates light application area over layer 2/3 (L2/3) with recording electrodes placed in L2/3 and L5. RF = Rhinal Fissure. B) Example L2/3 extracellular responses obtained during a 500 ms light ramp (left) and a 1500 ms ramp stimulus (right) in control conditions (black, $N = 32$), in the presence of AMPA, NMDA, and $GABA_A$ receptor antagonists (green, N = 32), and in the presence of TTX/Cd^{2+} to block action potentials (AP, yellow, $N = 11$). Red lines indicate analysis windows. C) Average power spectra of L2/3 activity recorded in the 3 recording conditions for both 500 and 1500 ms stimuli. Each plot depicts the mean (thick line) and SEM (thin lines). Blue shaded areas indicate "gamma" (30–100 Hz) and "high" (200–600 Hz) frequency bands. D,E) Scatter plots for average L2/3 power during the 500 ms ramp for the gamma range (D) and high-frequency range (E). Note that the means are the linear means plotted on a log scale. A 2-way rmANOVA was performed on data in (D) and (E) (drug treatment x frequency, repeated measures for the latter; For drug, $F(2,71) = 48$, $p < .0001$; for frequency, $F(1,71) = 388$, $p < .0001$; for interaction, $F(2,71) = 125.1$,$p < .0001$) and asterisks indicate multi-comparison statistical results. Scale bars in B = 250 ms, 200 μV. $^{**}p < .01$; $^{****}p < .0001$.

Activity was clearly evoked in WT recordings and power spectra were calculated (Fig. 1B,C; black; $N = 32(6)$, 32 slices obtained from 6 mice). To isolate the component dependent on synaptic transmission, we applied ionotropic receptor antagonists for AMPA-Rs (20 μM DNQX), NMDA-Rs (5 μM CPP), and $GABA_A$-Rs (100 μM Picrotoxin) in the same recordings (Fig. 1B, green). Power in the gamma band was dramatically decreased by 98% (Fig. 1D), while in the high-frequency band, power was only decreased by 43% (Fig. 1E). In a 2-way rmANOVA analysis restricted to only these control and antagonist wash-in experiments (only black and green data in Fig. 1D,E; ANOVA described in Fig. 1), this greater block of gamma band power is further supported by the highly significant interaction term ($F(1,61) = 233$, $p < .0001$). These results are consistent with action potentials being a large contributor to signals in the high-frequency band while ionotropic receptor-mediated synaptic transmission is required for almost all power in the gamma frequency range. The results are also consistent with the known synaptic basis of gamma oscillations (Wang and Buzsaki, 1996).

While we focused on activity in L2/3, we also simultaneously recorded from layer 5 (L5) in these same receptor antagonist experiments. Action potential firing in L5 was decreased by 88% with antagonist application, indicating that L5 activation was more dependent on synaptic transmission which is consistent with the lack of light applied to L5 and the excitatory projection from L2/3 to L5 (Supp. Data, *Dependence of L5*).

To determine the component in L2/3 contributed by our artificial introduction of ChR2-mediated currents, we performed a separate set of experiments in the presence of TTX (1 μM) and Cd^{2+} (300 μM) to block action potentials, Ca^{2+} currents, and neurotransmitter release (Fig. 1, yellow, $N = 11(4)$). Although we did not block metabotropic receptors, we assume that the signal evoked by light in these circumstances is largely due to ChR2-mediated currents. This manipulation largely eliminated power in both the gamma and high-frequency bands (99.6% and 96% reduction, respectively; Fig. 1D,E). Therefore, only 1–4% of remaining activity originated from either recording noise or ChR2-induced currents. The loss of high-frequency power after blocking action potentials, and its preservation while blocking postsynaptic ionotropic receptors is consistent with signals in the high-frequency band originating mainly from action potential firing. In summary, light evoked activity reveals a division into two components: a gamma band that is most tightly linked to synaptic transmission and a high-frequency band that is most tightly linked to action potential firing.

3.2. Local activation of L2/3 reveals hyperexcitability in Fmr1 KO local L2/3 circuits which propagates to L5

To investigate whether *Fmr1* KO slices exhibit increased responsiveness compared to WT slices, we performed simultaneous recordings in L2/3 and L5 while stimulating L2/3 with brief, 10 ms light pulses ($N = 43(8)$, 39(7); Fig. 2A). Using this recording configuration, we measured "locally" activated L2/3 responses as well as activity that propagated from L2/3 to L5. In separate control experiments using intracellular recordings, the currents induced in individual L2/3 neurons were no different between WT and *Fmr1* KO slices (Supp. Fig. 1). Therefore, this experimental protocol was appropriate for comparing excitability between these 2 genotypes.

We applied a high-pass filter (300 Hz lower cut-off, Fig. 2B) and rectification to make time-domain response measurements, and as indicated above, this resulted in a measurement of activity most linked to action potential firing. We chose this approach because lower frequencies were largely contaminated by ChR2-mediated currents with brief light application. At light intensities where robust activity was evoked, local L2/3 response strength (described in methods) was greater in *Fmr1* KO slices - ranging from a 30% to 101% increase (Fig. 2C). Responses in L5 showed a similar increase (Fig. 2G). With application of 6 stimuli in rapid sequence (0.5 and 3 Hz), no change in habituation was observed (Supp. Fig. 2). These data indicate that both L2/3 and L5 were hyperexcitable, and that this hyperexcitability involves increased action potential firing.

To resolve the time windows in which the increased responses exist in the *Fmr1* KO slices, we analyzed a superset of L2/3 responses by adding data from another identical experiment (total $N = 75(14)$, 70(13); controls from Fig. 7B added. Only 0.8 mW/mm^2 intensity. Fig. 2D,H). For both L2/3 and L5 recordings, the increased responses in *Fmr1* KO slices were most pronounced and only detectable within the first 30 ms after light onset (Fig. 2D,H; Supp. Fig. 3; Supp. data in *Time Course of Responses to 10 ms Pulses*).

While we demonstrate that light activation of L2/3 results in hyperactivity in L5 networks in the *Fmr1* KO, it is not clear whether L5 circuits are intrinsically hyperexcitable or simply responding to increased input from L2/3. To address this, we applied the same 10 ms light protocol to L5 and recorded only from L5 ($N = 41(7)$, 46(8); Fig. 2I). We found no differences in responses between WT and *Fmr1* KO slices (Fig. 2K,L). Therefore, while L2/3 is intrinsically hyperexcitable, L5 is not. We performed the same experiments in L5 using a different Cre-line that also expresses Cre-recombinase in cortical excitatory neurons (Nex-Cre) (Goebbels et al., 2006). Again, no differences were observed at either 3 weeks of age ($N = 40(7)$, 45(8)) or 5 weeks of age ($N = 36(7)$, 39(7)) (data not shown).

Next, we determined whether increased activity in *Fmr1* KO slices is maintained as long as experimental drive is applied. We employed 500 and 1500 ms light ramps. This might be considered analogous to "resting state" conditions during waking states where cortical activation is maintained but has no clear response to sensory stimuli. All experiments were performed with 0.35 mW/mm^2 light intensity ($N = 28(6)$, 35(7)).

We first examined responses in the time-domain by comparing average activity during light presentation (Fig. 3A,D). For the 500 ms ramp, the average activity in L2/3 during light application was 34% greater in the *Fmr1* KO slices (Fig. 3B). Similarly, the L5 responses were increased by 42% (Fig. 3E). Activity was also higher in *Fmr1* KO slices when observed during the 1500 ms ramp (Supp. Table 1). No differences in L5 response strength were observed when 500 ms ramp stimuli were applied directly to L5 (Supp. Table 2) which confirms the layer specificity of hyperexcitability. To determine how this difference persevered throughout the light application, we pooled these data with controls from another experiment (in Fig. 7) to obtain a data superset ($N = 60(13)$, 66(14)). We found that increased activity in the *Fmr1* KO slices was most prominent within the first 50 ms of the light ramp, but the increase was still trending for the rest of the light application time (Fig. 3C,F; Supp. Fig. 4; Supp. data in *Time Course of Responses to Longer Ramps*).

3.3. Local L2/3 and L5 circuits of Fmr1 KO display enhanced activity in the gamma and high-frequency ranges

In these same experiments employing the longer duration light ramps, we examined activity in the frequency domain by calculating power spectra (same recordings as in Fig. 3B, N = 28(6), 35(7)). We focused on the 30–100 Hz (gamma) and 200–600 Hz (high-frequency) bands. For L2/3, we observed 117% and 75% increases in power for gamma and high-frequency bands, respectively, during the 500 ms ramp (Fig. 4A,B). For L5, increases of 230% and 120% were found for the gamma and high-frequency bands, respectively (Fig. 4E,F). Results were the same for the longer 1500 ms ramp (data not shown). Increased power in *Fmr1* KO slices was most salient during the first 500 ms after light ramp onset (Supp. Figs. 5,6; Supp. data in *Time Course of Responses to Longer Ramps*). These changes were also layer-specific, since no differences were detected in L5 when directly stimulated (Supp. Table 2). In summary, local cortical networks in the *Fmr1* KO slices have more internally generated power in both gamma and high frequency bands when activated through L2/3.

To better examine these changes in signal power, we again used the

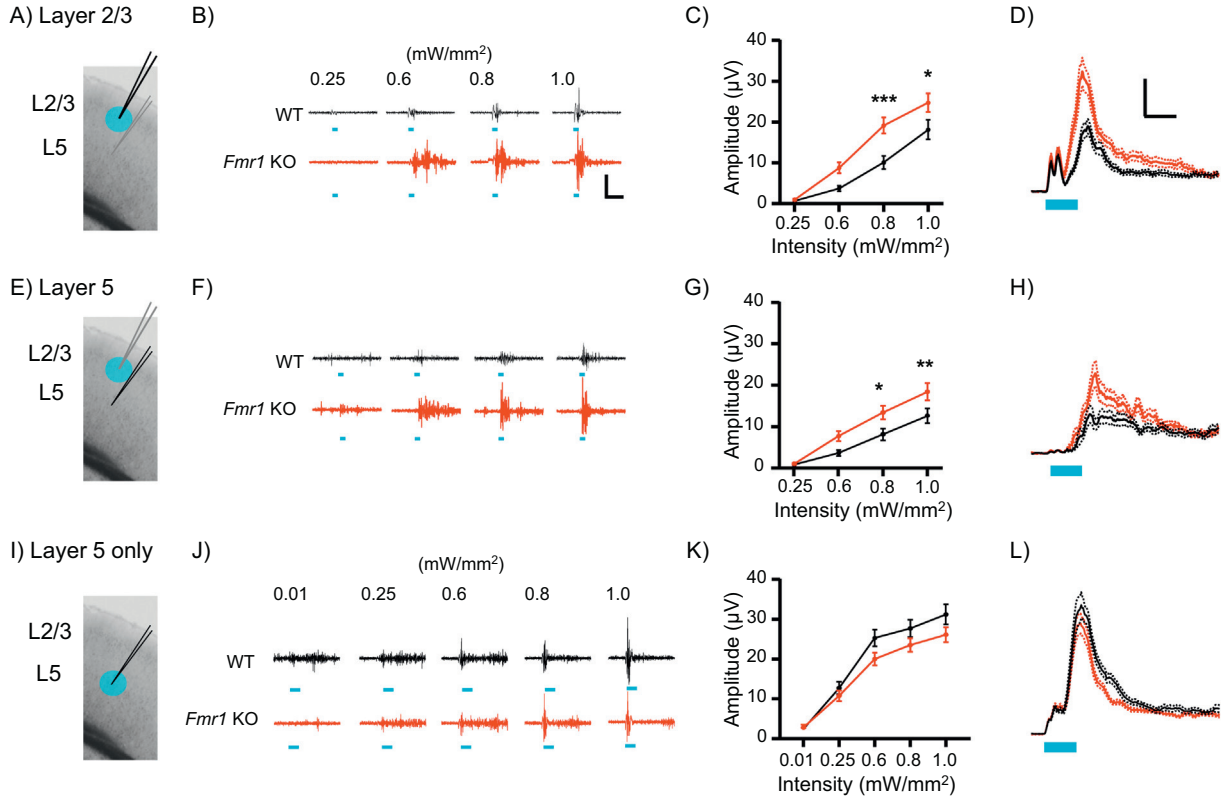

Fig. 2. Responses are enhanced in *Fmr1* KO slices with light activation of L2/3, but not with activation of L5. A,E,I) Configuration of experiments for simultaneous recordings (A,E; $N = 43,39$; WT,KO) and single L5 recordings (I; $N = 41,46$). Blue indicates light application area. The black recording pipette indicates the origin of data plotted in that row. B,F,J) Example responses from WT (black) and *Fmr1* KO slice (red) to 10 ms light pulses at different intensities. C,G,K) Average amplitude plotted as a function of stimulation intensity. A 2-way rmANOVA was applied to each data set (genotype x light intensity) and responses were significantly greater in *Fmr1* KO slices in (C) ($F(1,80) = 9.3$, $p < .01$) and (G) ($F(1,80) = 6.5$, $p < .05$). D,H,L) Overlaid rectified average traces from WT and *Fmr1* KO slices. Solid and dashed lines indicate mean and SEM, respectively, of responses collected at an intensity of 0.8 mW/mm^2 (for D and H, control data from Fig. 7 added; $N = 75,70$). Scale bars in B apply to B,F,J. 50 ms,100 μV. Scale bars in D apply to D,H,L: 10 ms,10 μV. Asterisks indicate multi-comparison statistical results. *$p < .05$; **$p < .01$; ***$p < .001$; ****$p < .0001$.

same superset of recordings (total N = 60(13), 66(14); controls in Fig. 7 added). For L2/3, the increase in power was equal in the two frequency bands. This was based on measuring the ratio of total power in the 30–100 Hz range to that in the 200–600 Hz range (gamma/high-frequency). For both 500 and 1500 ms light application, this ratio was unchanged between WT and *Fmr1* KO slices (Fig. 4C; only shown for 500 ms). Therefore, the power increases in L2/3 were fairly uniform over the range of frequencies examined. On the other hand, there was a 37% and 43% increase in the ratio of gamma/high-frequency power in L5 of *Fmr1* KO slices (500 and 1500 ms, ramps, respectively) indicating a bigger relative increase in gamma power (Fig. 4G, only shown for 500 ms). This selective increase in L5 gamma frequencies was also observed using power spectra normalized to total power (Fig. 4D,H) which showed a 25% increase in *Fmr1* KO slices ($p < .01$, 2-way rmANOVA as described in Fig. 4).

3.4. Activity in L2/3 and L5 display enhanced synchrony of gamma frequencies in Fmr1 KO slices

In this same superset, we examined the normalized cross-correlogram between activity in L2/3 and L5 to determine if synchrony between the two layers is altered in the *Fmr1* KO (Fig. 5A) (Deans et al., 2001; Gibson et al., 2008). For the raw traces, it was difficult to detect changes in the normalized cross-correlation. But differences emerged when we focused on synchrony in the gamma range by applying a 30–100 Hz bandpass filter to raw traces.

While we observed no difference in synchrony during the 500 ms ramp, there was a striking effect observed during the 1500 ms ramp (Fig. 5B). The amplitude of the peak to right trough of the average normalized cross correlation was 43% higher in the *Fmr1* KO slices (Fig. 5C). The timing of the peaks and troughs were not detectably different in *Fmr1* KO slices. For example, the "center" peaks for WT and *Fmr1* KO correlations both occurred at −2 ms indicating that, on average, correlated activity in layer 5 preceded that in layer 2/3 by about 2 ms. Using the same analysis, we also observed an increase in high frequency band synchrony (200–600 Hz) in *Fmr1* KO slices, but the synchrony observed in this band was only about 15% of the magnitude observed for the gamma synchrony (Supp. Fig. 7).

To test whether the correlation differences were due to increased activity levels in the *Fmr1* KO slices, we limited our analysis to recordings in which both L2/3 and L5 activity were within the 20–80% population distribution of the response amplitudes derived from our time-domain analysis ($N = 25(5), 23(5)$; 20–80% limits based on the pooled WT and *Fmr1* KO population). Unlike the complete data set, this restricted population had no differences in average response amplitude. Even with this limited set, the increased gamma synchrony in *Fmr1* KO networks was observed indicating that this effect was independent of the amount of activity in the 2 layers (Fig. 5D). In summary, these data show that internally generated gamma activity in cortical networks are more synchronous between layers in the *Fmr1* KO slices.

3.5. Modulation at a gamma frequency (30 Hz) reveals hyperexcitability and increased synchrony of circuits in the Fmr1 KO

EEG studies in patients and mice have shown that the ability of sensory input to phase-lock cortical activity is decreased in the gamma

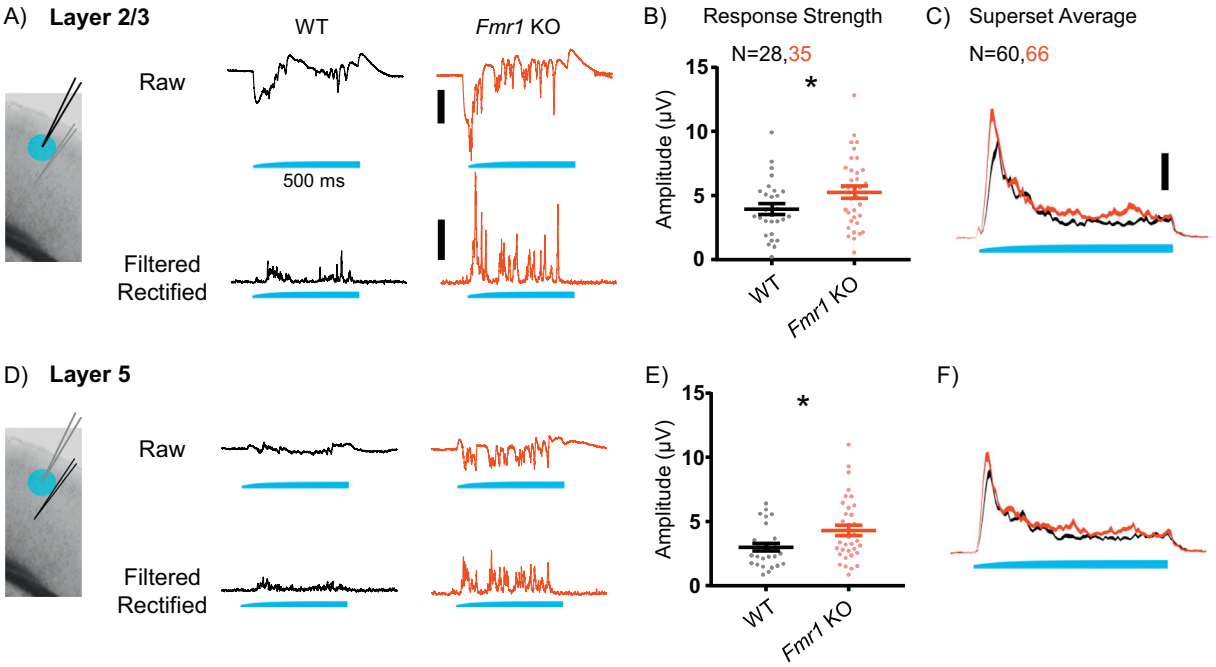

Fig. 3. Enhanced excitability to sustained circuit activation in *Fmr1* KO slices. A,D) Example traces simultaneously recorded from L2/3 and L5 in response to a 500 ms ramp illumination of L2/3 (WT = black, *Fmr1* KO = red). Both raw traces (*top*) and high-pass filtered and rectified (*bottom*) versions are shown. B,E) Scatter plots of average response amplitude during light application derived from rectified traces (N = 28,35). C,F) Averages of filtered and rectified traces (data pooled with control data from Fig. 7 resulting in N = 60,66). Thickness of traces is the SEM. Scale bars: A = 400 μV (*top*) and 4 μV (*bottom*), C = 10 μV. Bars in A and C apply to D and F. M-W *t*-tests, *$p < .05$.

frequency band (Ethridge et al., 2016; Ethridge et al., 2017). To determine the role auditory cortex may play in this, we performed experiments where we applied a light stimulus to L2/3 in the form of a 30 Hz sinewave of increasing amplitude (N = 25(5), 25(5), Fig. 6A,B). In unfiltered traces, the oscillation generated by ChR2-mediated currents was clearly observed in both L2/3 and L5. To avoid this contamination, we applied the high-pass filtering and rectification to restrict analysis to signals originating mostly from action potential firing. In this way, we can measure the 30 Hz modulation of action potential firing (note that this 30 Hz modulation is undetectable in the power spectra without the rectification step).

We found that the power in the 29–31 Hz band was 155% stronger in *Fmr1* KO slices compared to WT (Fig. 6C,D). In L5, a statistical trend of a 124% increase was observed (Fig. 6E, $p = .1$, M-W *t*-test). In these same recordings, we also applied the normal 1500 ms light ramp where the differences observed were not as robust as with the sinewave light modulation. First, in this normal ramp, there was no detectable difference in 29–31 Hz power. Second, there was only a trend for a 40% increase in the average time domain amplitude in the *Fmr1* KO (p = .1, M-W t-test). Therefore, the sinewave modulation of activity revealed a more pronounced and consistent phenotype in *Fmr1* KO slices compared to the absolute levels of activity evoked. In other words, the hyperexcitable phenotype appears to be enhanced with externally applied 30 Hz modulation.

With the same high-pass filtered and rectified traces, we measured the synchrony between L2/3 and L5 during the 30 Hz modulation by obtaining normalized cross-correlograms. Before performing this correlation analysis, we applied an additional 20–40 Hz band-pass filter to the traces to focus on the synchronization around the modulation frequency. We observed a 52% increase in the normalized cross-correlogram amplitude (Fig. 6F,G). This is consistent with the increased synchrony observed during the ordinary light ramps. In summary, these data show that when L2/3 networks in the *Fmr1* KO slices are externally driven at a gamma frequency, they show increased power and synchrony at that frequency.

3.6. Enhanced high-frequency activity of Fmr1 KO L2/3 circuits is independent of fast, ionotropic synaptic transmission with maintained circuit activation

We determined the extent to which hyperactivity in L2/3 of *Fmr1* KO slices is independent of the 3 main ionotropic postsynaptic receptor types – AMPA-Rs, NMDA-Rs, and $GABA_A$-Rs. We recorded from slices first in control ACSF and again after 15 min in three antagonists targeting these postsynaptic receptors – DNQX, CPP, and picrotoxin, respectively (Fig. 7A). In both WT and *Fmr1* KO slices, approximately 55% of the high-frequency signal remained after postsynaptic synaptic receptor blockade (averaging over all light applications - 10, 500, 1500 ms).

Examining activity measured in the time domain indicates that effects were dependent on the duration of the light stimulus. For the 10 ms light application, we applied increasing intensities as in earlier figures (Fig. 7B). While we reproduced our genotypic effect in control ACSF where L2/3 responses were bigger in the *Fmr1* KO slices, this was not observed with the antagonists applied. Therefore, postsynaptic receptor blockade removed the increased responsiveness of the *Fmr1* KO slices (Fig. 7B).

But for the longer duration ramp stimuli, the antagonists did not alter the hyperexcitability in L2/3 of *Fmr1* KO slices (N = 32(7), 31(7)). Power in the gamma band was virtually eliminated and not analyzed (See Fig. 1C). In the time-domain, amplitudes measured during blockade were still greater in *Fmr1* KO slices (Fig. 7C). Similarly, power in the high-frequency band remained greater in the antagonists (Fig. 7C). The same results for time-domain and frequency-domain were also observed for the 1500 ms light ramp (data not shown). Therefore, hyperexcitability is independent of synaptic transmission only with maintained drive suggesting a mechanism involving intrinsic ion conductances that is slow to engage.

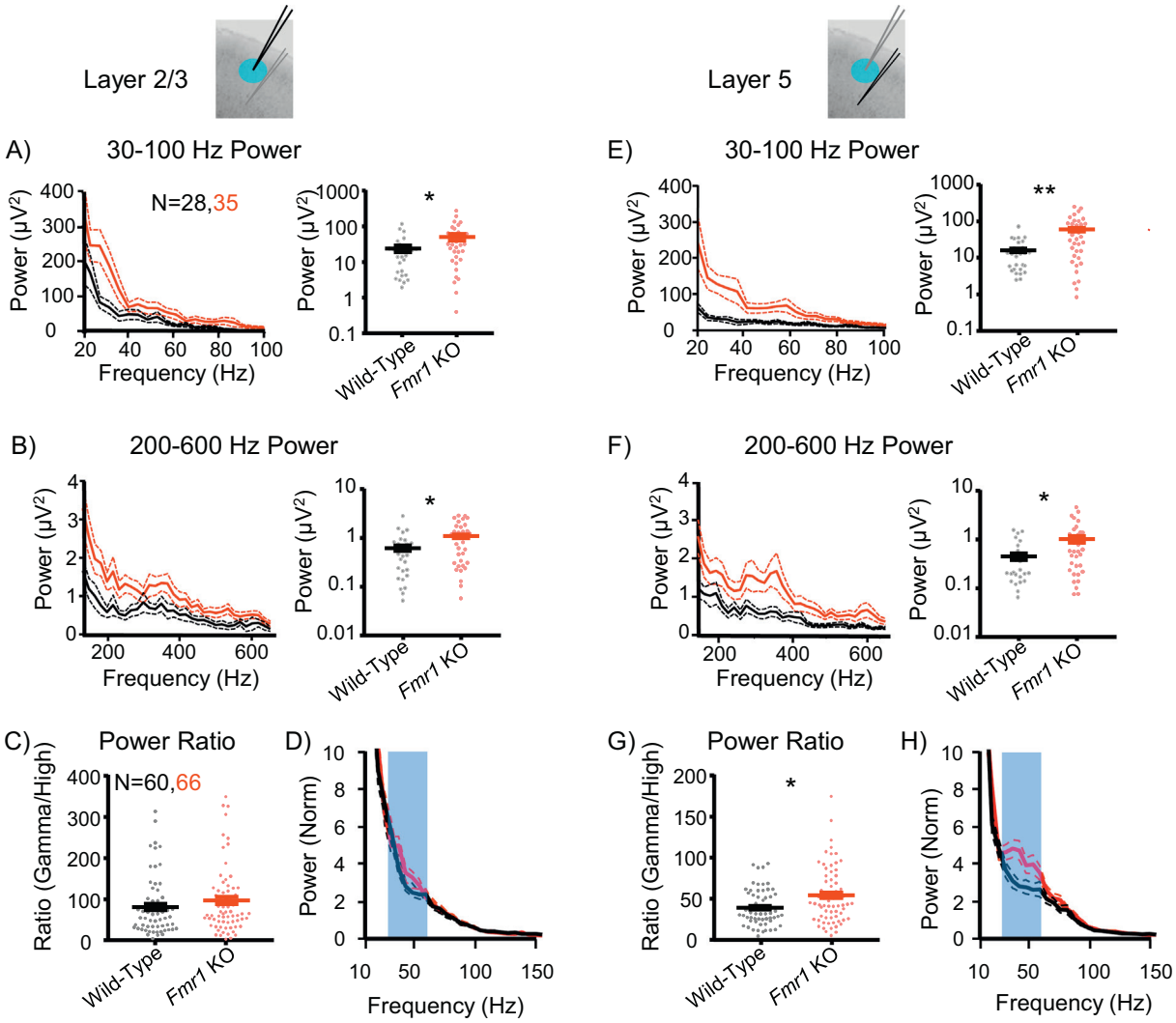

Fig. 4. Higher power in gamma (30–100 Hz) and high-frequency (200–600 Hz) bands in L2/3 and L5 in *Fmr1* KO. Analysis is performed on data from the same simultaneous recording experiments illustrated in Fig. 3: L2/3 (A-D) and L5 (*E*-H) (N = 28,35). Power spectra are plotted with mean (solid) ± SEM (dashed line). Black = WT, Red = *Fmr1* KO. A 2-way rmANOVA was performed on L2/3 data and L5 data separately (genotype x frequency band, latter repeated measures), and each indicated a significant effect for genotype ($F(1,61) = 5.9$, $p < .05$; $F(1,61) = 7.2$, $p < .01$). For both L2/3 and L5, power is greater in *Fmr1* KO slices for the 30–100 Hz band (A,E) and the 200–600 Hz band (B,F). C,G) *Fmr1* KO slices show a higher ratio of 30–100 Hz/200–600 Hz power in L5 but not L2/3. D,H) Normalized power spectra also reveal greater enhancement of 30–100 Hz power in L5 but not L2/3 (Blue highlights the 30–60 Hz range). Spectra were normalized to total power in 10–600 Hz window. Data in C,D and G,H include additional control data from Fig. 7 (resulting in N = 60,66). (A-C, E-G) and (D,H) based on 500 ms and 1500 ms light ramps, respectively. Asterisks in (A,B,E,F) indicate multi-comparison statistical results, and those in (C,G), M-W t-test results. *$p < .05$; **$p < .01$.

3.7. Acute lovastatin application does not normalize enhanced gamma power

Pathophysiology in FXS has been linked to excess activity of the extracellular signal-regulated kinase (ERK1/2) which is driven by the small GTPase Ras and MAP-ERK Kinase (MEK) (Osterweil et al., 2013; Osterweil et al., 2010). Lovastatin prevents activation of Ras (Kloog et al., 1999; Li et al., 2005), and is currently in clinical trials for FXS (https://clinicaltrials.gov/ct2/show/NCT02680379;NCT02642653; NCT02998151). Acute treatment (< 1 h) of lovastatin or inhibitors of MEK block audiogenic seizures and hyperexcitability of visual cortical circuits in *Fmr1* KO mice (Osterweil et al., 2013), suggesting that lovastatin may be a candidate therapeutic to correct auditory cortex circuit hyperexcitability that we observe in *Fmr1* KO slices.

To test this idea, we examined the ability of lovastatin to correct the enhanced light evoked responses by first measuring responses in normal ACSF and again after a 50 min incubation in lovastatin (50 μM, *N* = 35(6), 35(6)) (Fig. 8A). Some of the data were inconclusive (Supp. Fig. 8), but we observed 2 clear negative results. First, lovastatin did not correct the enhanced responses to brief light stimuli in local L2/3 of *Fmr1* KO slices (Fig. 8B). Second, lovastatin did not correct the increased gamma power observed in *Fmr1* KO slices in either L2/3 or L5 (Fig. 8C,D). Lovastatin decreased gamma for both genotypes, but based on control experiments with wash-in of vehicle, this decrease was not attributable to the drug (see Supp. Data, *Additional Lovastatin Data*). We also observed no effects of Lovastatin on interlayer synchrony (Supp. Fig. 9).

4. Discussion

4.1. Hyperactivity and increased gamma power in local cortical circuits

Robust changes in resting state and sound-evoked EEGs are observed in FXS patients, and these changes are remarkably conserved in the corresponding mouse model - the *Fmr1* KO. This cross-species conservation of neurophysiological phenotypes offers an exciting

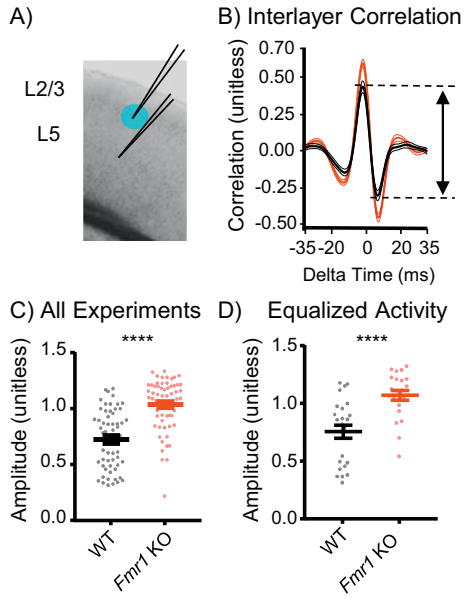

Fig. 5. Increased synchrony of gamma signals between L2/3 and L5 in *Fmr1* KO slices. Cross correlations between simultaneous L2/3 and L5 recordings (recordings pooled from experiments depicted in Figs. 4A-F and 7C-D; N = 60,66). A) The recording and light illumination configuration. B) Average normalized correlograms for traces that were first bandpass filtered between 30 and 100 Hz to focus on the interlayer coupling in the gamma band during the 1500 ms ramp. The average peak-to-trough amplitude is the measure of synchrony strength as indicated by the double arrow line. Black = WT, Red = *Fmr1* KO. Lines are Mean ± SEM. C) Peak-to-trough amplitudes are significantly higher in the *Fmr1* KO slices indicating greater interlayer coupling. D) After eliminating slices whose time-domain amplitudes were outside the 20–80% group of the distribution and thereby equalizing average amplitude, significant differences in correlogram amplitude remain. Asterisks indicate M-W t-test results. ****$p < .0001$.

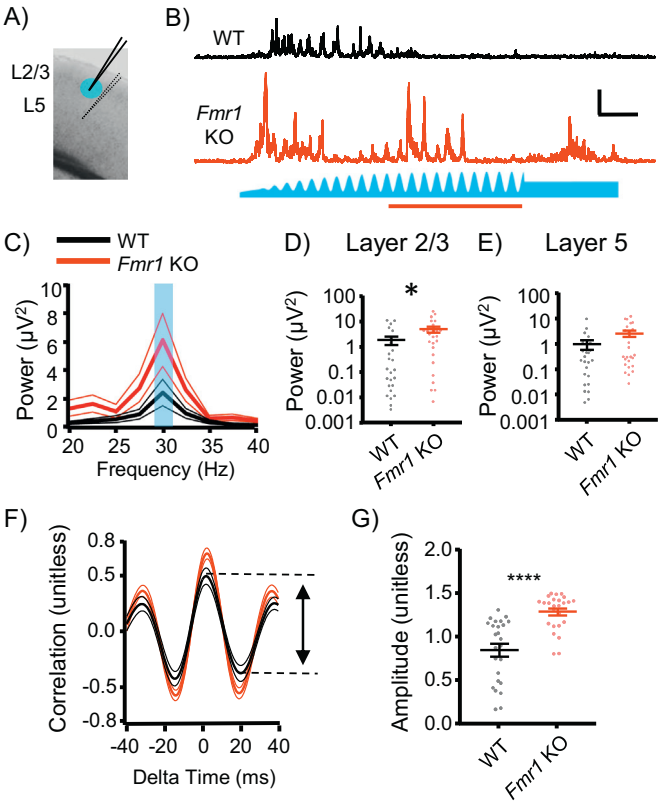

Fig. 6. Increased synchrony between L2/3 and L5 of *Fmr1* KO mice during 30 Hz modulation of light. A) The recording and light illumination configuration. B) Example traces of single responses (black = WT, red = *Fmr1* KO) to a light ramp with a ramping 30 Hz sinewave superimposed (illustrated in blue). Traces are high-pass filtered and rectified to focus on signals more tightly linked to action potential firing. Red line indicates the analysis window. C) Average power spectra during the sinewave stimulus. Thick and thin lines indicate mean and SEM., respectively (N = 25,25). D,E) Plots of power in the 29–31 Hz range (blue shaded region in C) reveal an increase in *Fmr1* KO slices in L2/3 (D) and a trending increase in L5 (E, p = .1). F) Average normalized cross-correlograms between L2/3 and L5. The arrow line indicates the peak-to-trough amplitude as the measure of synchrony strength. G) The peak-to-trough amplitudes are significantly higher in *Fmr1* KO slices. Scale bars in B = 100 ms, 25 μV. Asterisks indicate M-W t-test results. *p < .05, ****p < .0001.

opportunity to understand the circuit dysfunction in *Fmr1* KO mice and from this knowledge develop therapeutics that can be translated to patients. Towards this goal, we applied an optogenetic assay to probe excitability of local circuits in the auditory neocortex and to measure network activity that correlates with the EEG. We find that experimental activation of L2/3 circuits reveals circuit hyperexcitability in both L2/3 and L5 in the *Fmr1* KO mouse when focusing on signals closely linked to action potential firing. Furthermore, activated circuits in *Fmr1* KO slices have higher power across a broad range of frequencies (including gamma, 30–100 Hz) suggesting that synaptic activity is increased as well. Gamma power is especially enhanced in L5 *Fmr1* KO circuits. It remains unclear how this occurs, but we suggest 2 possibilities: 1) combined effects of changes in L2/3 and L5, or 2) a specific change in the functional properties of the L2/3 to L5 projection.

While hyperexcitability was observed in L5 with L2/3 light activation in *Fmr1* KO slices, this was not observed when L5 was directly activated indicating that hyperexcitability is layer specific depending on where the stimulation is applied. This finding is consistent with the idea that the increased activity observed in L5 with L2/3 light activation is due to the increased activity in L2/3 being projected onto L5 through its excitatory projection to L5.

We observe that circuit activity measured in the gamma range is more synchronized between L2/3 and L5 in the *Fmr1* KO. We observe this for both synaptically linked activity (30–100 Hz, see Fig. 5) and for action potential-linked activity driven by 30 Hz light modulation (see Fig. 6). This is similar to the increased synchronization of low frequency events in L2/3 at early postnatal stages (P10–14) in the *Fmr1* KO (Goncalves et al., 2013), but it is in contrast to the decreased synchrony of inhibitory synaptic currents measured among layer 4 neurons during persistent activity states in somatosensory barrel structures of the cortex (Gibson et al., 2008). These differences in synchrony alterations in the *Fmr1* KO may relate to specific intra-layer and inter-layer interactions in the cortex.

Altered function of ion channels that regulate intrinsic excitability are suggested to contribute to hyperexcitability of *Fmr1* KO cortical circuits, such as HCN, BK, and others (Zhang et al., 2014; Deng and Klyachko, 2016; Bianchi et al., 2009). Consistent with these studies, we observe hyperexcitability and increased power in the high-frequency (200–600 Hz) band in *Fmr1* KO circuits that persisted with blockade of fast synaptic transmission (with maintained activation of L2/3). These data suggest that more action potentials were elicited during light application and are consistent with increases in intrinsic excitability of individual neurons in *Fmr1* KO circuits previously reported (Zhang et al., 2014; Gibson et al., 2008). One working hypothesis based on these data is that increased power in the gamma band results from this increase in intrinsic excitability of individual neurons driving an increase in synaptic activity. Indeed, computational studies indicate that increased excitation in a network can increase the amount of gamma oscillatory power (Wang and Buzsaki, 1996). These experiments cannot rule out a role for metabotropic postsynaptic receptors in the increased intrinsic excitability since their role was not examined. Interestingly,

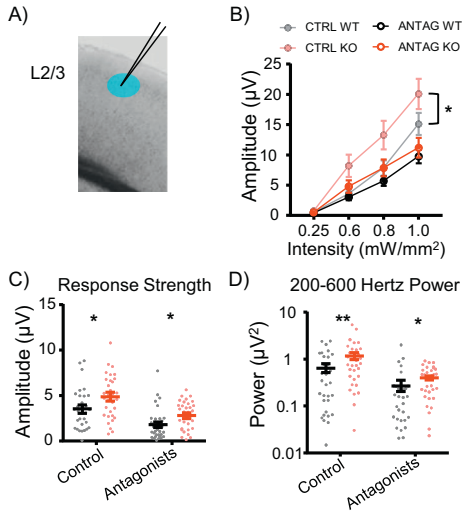

Fig. 7. Blocking ionotropic glutamate and GABA receptors still reveals a power increase in the high-frequency band in the *Fmr1* KO slices during sustained circuit activation. A) Experimental scheme indicating L2/3 recording and light application. B) Average response amplitudes to 10 ms light pulses in control ACSF (unsaturated colors) and in ACSF containing the ionotropic receptor antagonists (saturated colors) (N = 49,47). While response amplitudes were greater in *Fmr1* KO in control ACSF, amplitudes were equalized with antagonist application (based on 3-way rmANOVA, genotype x intensity x drug treatment, with latter 2 repeated measures; genotype x drug treatment interaction, F = 3.4, p < .05). C) For 500 ms ramps, increased amplitudes measured in the time domain remained higher in *Fmr1* KO slices after application of the antagonists. D) Similarly, the increase in average power in the 200–600 Hz band observed in *Fmr1* KO slices remained after antagonist application. For (C,D), a 2-way rmANOVA was applied for data in each plot with drug treatment the repeated factor. Asterisks indicate multi-comparison statistical results. *p < .05, **p < .01.

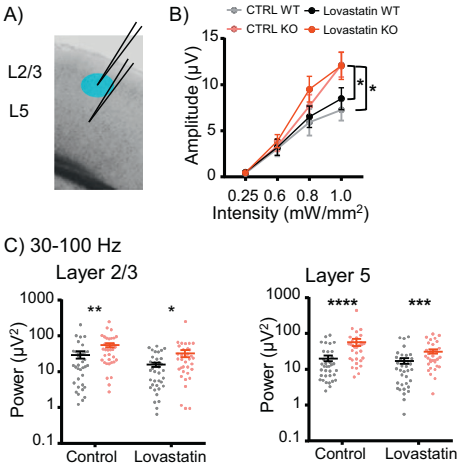

Fig. 8. Differences in excitability and gamma power remain after application of lovastatin. A) Experimental scheme indicating recordings and light application. B) Response amplitudes to 10 ms light pulses in L2/3 recordings. Traces were first obtained in control ACSF (unsaturated colors) and then in the presence of 50 μM lovastatin (saturated colors). Based on a 3-way ANOVA (genotype × intensity × drug treatment, repeated measures for the last 2 factors), *Fmr1* KO slices had larger responses in control ACSF and in lovastatin (genotype factor, F = 12.6, p < .0001; genotype x drug interaction, F = 0.001, p = .98) (N = 35,34). C) The power in the 30–100 Hz band during the 500 ms ramp stimulus measured in WT (black) and *Fmr1* KO slices (red) is plotted for L2/3 (left) and L5 (right). Data are from the 500 ms ramp stimulus. The *Fmr1* KO slices had higher power both in control ACSF and with lovastatin added. For (C), a 2-way rmANOVA was applied for data in each plot with drug treatment the repeated factor. In addition to the multi-comparison analysis in (C), the lack of a specific effect by Lovastain is also indicated by insignificant interaction terms (L2/3, F(1,67) = 0.79, p = .38; L5, F(1,67) = 0.92,p = .34). Asterisk indicate multi-comparison statistical results. *p < .05, **p < .01, ***p < .001, ****p < .0001.

this increase in high-frequency power in synaptic blockers was observed with long (500–1500 ms), but not short (10 ms) light application suggesting that a relatively slow onset (> 10 ms) mechanism drives increases in intrinsic excitability in *Fmr1* KO neurons.

4.2. Linking to in vivo changes

In primary sensory cortices of the *Fmr1* KO mouse, both spontaneously occurring activity and activity evoked by sensory stimulation are enhanced (Zhang et al., 2014; Goncalves et al., 2013), and this includes auditory cortex (Rotschafer and Razak, 2013; Lovelace et al., 2016). Recent EEG studies investigating the auditory system in FXS patients report similar properties – including increased "resting gamma" power (Knoth et al., 2014; Wang et al., 2017; Van der Molen et al., 2012; Ethridge et al., 2017). It has not been clear if cortical circuits could play a role in these increases or if the increases reflect altered synaptic drive from other presynaptic brain structures. Our results indicate that neocortex likely plays a role in these systems level alterations.

Based on our findings that both gamma power and gamma synchrony are enhanced in *Fmr1* KO networks, we hypothesize that the enhancement of resting gamma in the EEG may be explained as follows. The strength of an EEG signal depends on both signal strength generated by local networks and on synchrony among networks (Luck, 2005). Therefore, increased gamma produced by local networks together with increased inter-layer synchronization may combine to enhance the gamma power in the EEG.

In addition to enhanced resting state gamma power, auditory stimuli have a reduced ability to synchronously drive cortical networks at gamma frequencies in both *Fmr1* KO mice and FXS patients (Ethridge et al., 2017; Lovelace et al., 2018). It was hypothesized that the higher background gamma power acts as noise that impedes the gamma frequency drive of auditory stimuli. Our data is consistent with this hypothesis in the sense that the increased gamma power occurring in local circuits may insert noise into a signal generated by stimulus driven activity. But in addition, our data suggest that the increased interlayer synchronization may make cortical networks more resistant to external stimulus synchronization by increasing the stability of "internal" gamma frequencies. Therefore, greater sensory input would be required to overcome the "internal" gamma state and to synchronize cortical activity.

It should be stressed that our findings are strictly correlational and future experiments will be required to reasonably test the hypotheses that we have proposed. For example, analogous local circuit activation experiments should be performed *in vivo* to determine if our results are found in the more complete and intact network. Also, *Fmr1* deletion in specific cortical layers using existing Cre lines may better isolate particular circuits to EEG changes *in vivo*.

In summary, the link of our data to the observed changes *in vivo* remains correlational, but the similarity in changes of local cortical circuit function to that observed at the systems level are compelling. Our study points to the importance of a circuit level, *in vitro* approach as part of a strategy to understand brain function changes in FXS.

Acknowledgements

We thank Simon Ammanuel, Manasa Sarma, and Bianca Walker for technical assistance. This work was supported by a grant from the NIH (U54HD082008; JRG, KMH).

Disclosures

The authors declare that they have no competing interests.

Appendix A. Supplementary data

Supplementary data to this article can be found online at https://doi.org/10.1016/j.nbd.2019.01.002.

References

Abrahams, B.S., Geschwind, D.H., 2008. Advances in autism genetics: on the threshold of a new neurobiology. Nat. Rev. Genet. 9, 341–355.

Bakker, D.B., 1994. Fmr1 knockout mice: a model to study fragile X mental retardation. The Dutch-Belgian Fragile X consortium. Cell 78, 23–33.

Baranek, G.T., Roberts, J.E., David, F.J., Sideris, J., Mirrett, P.L., Hatton, D.D., et al., 2008. Developmental trajectories and correlates of sensory processing in young boys with fragile X syndrome. Phys. Occup. Ther. Pediatr. 28, 79–98.

Bassell, G.J., Warren, S.T., 2008. Fragile X syndrome: loss of local mRNA regulation alters synaptic development and function. Neuron 60, 201–214.

Berry-Kravis, E., 2002. Epilepsy in fragile X syndrome. Dev. Med. Child Neurol. 44, 724–728.

Bianchi, R., Chuang, S.C., Zhao, W., Young, S.R., Wong, R.K., 2009. Cellular plasticity for group I mGluR-mediated epileptogenesis. J. Neurosci. 29, 3497–3507.

Boyden, E.S., Zhang, F., Bamberg, E., Nagel, G., Deisseroth, K., 2005. Millisecond-time-scale, genetically targeted optical control of neural activity. Nat. Neurosci. 8, 1263–1268.

Brennan, F.X., Albeck, D.S., Paylor, R., 2006. Fmr1 knockout mice are impaired in a leverpress escape/avoidance task. Genes Brain Behav. 5, 467–471.

Castren, M., Paakkonen, A., Tarkka, I.M., Ryynanen, M., Partanen, J., 2003. Augmentation of auditory N1 in children with fragile X syndrome. Brain Topogr. 15, 165–171.

Contractor, A., Klyachko, V.A., Portera-Cailliau, C., 2015. Altered neuronal and circuit excitability in fragile X syndrome. Neuron 87, 699–715.

Cruikshank, S.J., Rose, H.J., Metherate, R., 2002. Auditory thalamocortical synaptic transmission in vitro. J. Neurophysiol. 87, 361–384.

Darnell, J.C., Klann, E., 2013. The translation of translational control by FMRP: therapeutic targets for FXS. Nat. Neurosci. 16, 1530–1536.

Darnell, J.C., Van Driesche, S.J., Zhang, C., Hung, K.Y., Mele, A., Fraser, C.E., et al., 2011. FMRP stalls ribosomal translocation on mRNAs linked to synaptic function and autism. Cell 146, 247–261.

Deans, M.R., Gibson, J.R., Sellitto, C., Connors, B.W., Paul, D.L., 2001. Synchronous activity of inhibitory networks in neocortex requires electrical synapses containing connexin36. Neuron 31, 477–485.

Deng, P.Y., Klyachko, V.A., 2016. Genetic upregulation of BK channel activity normalizes multiple synaptic and circuit defects in a mouse model of fragile X syndrome. J. Physiol. 594, 83–97.

Ethridge, L.E., White, S.P., Mosconi, M.W., Wang, J., Byerly, M.J., Sweeney, J.A., 2016. Reduced habituation of auditory evoked potentials indicate cortical hyper-excitability in Fragile X syndrome. Transl. Psychiatry 6, e787.

Ethridge, L.E., White, S.P., Mosconi, M.W., Wang, J., Pedapati, E.V., Erickson, C.A., et al., 2017. Neural synchronization deficits linked to cortical hyper-excitability and auditory hypersensitivity in fragile X syndrome. Mol Autism. 8, 22.

Gibson, J.R., Bartley, A.F., Hays, S.A., Huber, K.M., 2008. Imbalance of neocortical excitation and inhibition and altered UP states reflect network hyperexcitability in the mouse model of fragile X syndrome. J. Neurophysiol. 100, 2615–2626.

Goebbels, S., Bormuth, I., Bode, U., Hermanson, O., Schwab, M.H., Nave, K.A., 2006. Genetic targeting of principal neurons in neocortex and hippocampus of NEX-Cre mice. Genesis 44, 611–621.

Goncalves, J.T., Anstey, J.E., Golshani, P., Portera-Cailliau, C., 2013. Circuit level defects in the developing neocortex of Fragile X mice. Nat. Neurosci. 16, 903–909.

Hagerman, R.J., Berry-Kravis, E., Kaufmann, W.E., Ono, M.Y., Tartaglia, N., Lachiewicz, A., et al., 2009. Advances in the treatment of fragile X syndrome. Pediatrics 123, 378–390.

Hays, S.A., Huber, K.M., Gibson, J.R., 2011. Altered neocortical rhythmic activity states in Fmr1 KO mice are due to enhanced mGluR5 signaling and Involve changes in excitatory circuitry. J. Neurosci. 31, 14223–14234.

Kloog, Y., Cox, A.D., Sinensky, M., 1999. Concepts in ras-directed therapy. Expert Opin. Investig. Drugs 8, 2121–2140.

Knoth, I.S., Vannasing, P., Major, P., Michaud, J.L., Lippe, S., 2014. Alterations of visual and auditory evoked potentials in fragile X syndrome. Int. J. Dev. Neurosci. 36, 90–97.

Li, W., Cui, Y., Kushner, S.A., Brown, R.A., Jentsch, J.D., Frankland, P.W., et al., 2005. The HMG-CoA reductase inhibitor lovastatin reverses the learning and attention deficits in a mouse model of neurofibromatosis type 1. Curr. Biol. 15, 1961–1967.

Lovelace, J.W., Wen, T.H., Reinhard, S., Hsu, M.S., Sidhu, H., Ethell, I.M., et al., 2016. Matrix metalloproteinase-9 deletion rescues auditory evoked potential habituation deficit in a mouse model of Fragile X syndrome. Neurobiol. Dis. 89, 126–135.

Lovelace, J.W., Ethell, I.M., Binder, D.K., Razak, K.A., 2018. Translation-relevant EEG phenotypes in a mouse model of Fragile X syndrome. Neurobiol. Dis. 115, 39–48.

Luck, S.J., 2005. An Introduction to the Event-Related Potential Technique. MIT Press, Cambridge, MA.

Madisen, L., Mao, T., Koch, H., Zhuo, J.M., Berenyi, A., Fujisawa, S., et al., 2012. A toolbox of cre-dependent optogenetic transgenic mice for light-induced activation and silencing. Nat. Neurosci. 15, 793–802.

Miller, L.J., McIntosh, D.N., McGrath, J., Shyu, V., Lampe, M., Taylor, A.K., et al., 1999. Electrodermal responses to sensory stimuli in individuals with fragile X syndrome: a preliminary report. Am. J. Med. Genet. 83, 268–279.

Musumeci, S.A., Hagerman, R.J., Ferri, R., Bosco, P., Dalla Bernardina, B., Tassinari, C.A., et al., 1999. Epilepsy and EEG findings in males with fragile X syndrome. Epilepsia 40, 1092–1099.

Musumeci, S.A., Bosco, P., Calabrese, G., Bakker, C., De Sarro, G.B., Elia, M., et al., 2000. Audiogenic seizures susceptibility in transgenic mice with fragile X syndrome. Epilepsia 41, 19–23.

Nielsen, D.M., Derber, W.J., McClellan, D.A., Crnic, L.S., 2002. Alterations in the auditory startle response in Fmr1 targeted mutant mouse models of fragile X syndrome. Brain Res. 927, 8–17.

Osterweil, E.K., Krueger, D.D., Reinhold, K., Bear, M.F., 2010. Hypersensitivity to mGluR5 and ERK1/2 leads to excessive protein synthesis in the hippocampus of a mouse model of fragile X syndrome. J. Neurosci. 30, 15616–15627.

Osterweil, E.K., Chuang, S.C., Chubykin, A.A., Sidorov, M., Bianchi, R., Wong, R.K., et al., 2013. Lovastatin corrects excess protein synthesis and prevents epileptogenesis in a mouse model of fragile X syndrome. Neuron 77, 243–250.

Patel, A.B., Loerwald, K.W., Huber, K.M., Gibson, J.R., 2014. Postsynaptic FMRP promotes the pruning of cell-to-cell connections among pyramidal neurons in the L5A neocortical network. J. Neurosci. 34, 3413–3418.

Rojas, D.C., Benkers, T.L., Rogers, S.J., Teale, P.D., Reite, M.L., Hagerman, R.J., 2001. Auditory evoked magnetic fields in adults with fragile X syndrome. Neuroreport 12, 2573–2576.

Rotschafer, S., Razak, K., 2013. Altered Auditory Processing in a Mouse Model of Fragile X Syndrome. (submitted).

Schneider, A., Leigh, M.J., Adams, P., Nanakul, R., Chechi, T., Olichney, J., et al., 2013. Electrocortical changes associated with minocycline treatment in fragile X syndrome. J. Psychopharmacol. 27, 956–963.

Sinclair, D., Featherstone, R., Naschek, M., Nam, J., Du, A., Wright, S., et al., 2017. GABA-B agonist baclofen normalizes auditory-evoked neural oscillations and behavioral deficits in the Fmr1 knockout mouse model of fragile X syndrome. eNeuro 4.

Spencer, C.M., Alekseyenko, O., Serysheva, E., Yuva-Paylor, L.A., Paylor, R., 2005. Altered anxiety-related and social behaviors in the Fmr1 knockout mouse model of fragile X syndrome. Genes Brain Behav. 4, 420–430.

Van der Molen, M.J., Van der Molen, M.W., Ridderinkhof, K.R., Hamel, B.C., Curfs, L.M., Ramakers, G.J., 2011. Auditory and visual cortical activity during selective attention in fragile X syndrome: a cascade of processing deficiencies. Clin. Neurophysiol. 123, 720–729.

Van der Molen, M.J., Van der Molen, M.W., Ridderinkhof, K.R., Hamel, B.C., Curfs, L.M., Ramakers, G.J., 2012. Auditory change detection in fragile X syndrome males: a brain potential study. Clin. Neurophysiol. 123, 1309–1318.

Vong, L., Ye, C., Yang, Z., Choi, B., Chua Jr., S., Lowell, B.B., 2011. Leptin action on GABAergic neurons prevents obesity and reduces inhibitory tone to POMC neurons. Neuron 71, 142–154.

Wang, X.J., Buzsaki, G., 1996. Gamma oscillation by synaptic inhibition in a hippocampal interneuronal network model. J. Neurosci. 16, 6402–6413.

Wang, G.X., Smith, S.J., Mourrain, P., 2014. Fmr1 KO and fenobam treatment differentially impact distinct synapse populations of mouse neocortex. Neuron 84, 1273–1286.

Wang, J., Ethridge, L.E., Mosconi, M.W., White, S.P., Binder, D.K., Pedapati, E.V., et al., 2017. A resting EEG study of neocortical hyperexcitability and altered functional connectivity in fragile X syndrome. J. Neurodev. Disord. 9, 11.

Zhang, Y., Bonnan, A., Bony, G., Ferezou, I., Pietropaolo, S., Ginger, M., et al., 2014. Dendritic channelopathies contribute to neocortical and sensory hyperexcitability in Fmr1(-/y) mice. Nat. Neurosci. 17, 1701–1709.